AD_____

COOPERATIVE AGREEMENT NUMBER DAMD17-95-2-5003

TITLE: Collaborative Research and Support of Fitzsimmons Army Medical Center Defense Women's Health Research Program Projects

Subtitle: Simultaneous Transmission/Emission Protocol (STEP) for Attenuation Correction of Breast and Diaphragmatic Attenuation Artifacts During SPECT 99mTc-Sestamibi Myocardial Perfusion Scans in Patients without Coronary Artery Disease

PRINCIPAL INVESTIGATOR: Hugh Mulligan; Mike McBiles
Albert Lambert; Dennis Stroud
Royce K. Solano; Sun Yung Kim

CONTRACTING ORGANIZATION: Facilitators of Applied Clinical Trials
San Antonio, Texas 78216

REPORT DATE: September 1998

TYPE OF REPORT: Final

PREPARED FOR: U.S. Army Medical Research and Materiel Command
Fort Detrick, Maryland 21702-5012

DISTRIBUTION STATEMENT: Approved for public release;
distribution unlimited

REPORT DOCUMENTATION PAGE

Form Approved
OMB No. 0704-0188

1. AGENCY USE ONLY *(Leave blank)*	2. REPORT DATE	3. REPORT TYPE AND DATES COVERED
	September 1998	Final (1 Feb 95 - 30 Sep 98)

4. TITLE AND SUBTITLE
Subtitle: Simultaneous Transmission/Emission Protocol (STEP) for Attenuation Correction of Breast and Diaphragmatic Attenuation Artifacts During SPECT 99mTc-Sestamibi Myocardial Perfusion Scans in Patients without Coronary Artery Disease

5. FUNDING NUMBERS
DAMD17-95-2-5003

6. AUTHOR(S)
Hugh Mulligan; Mike McBiles
Albert Lambert; Dennis Stroud
Royce K. Solano; Sun Yung Kim

7. PERFORMING ORGANIZATION NAME(S) AND ADDRESS(ES)
Facilitators of Applied Clinical Trials
San Antonio, Texas 78216

8. PERFORMING ORGANIZATION REPORT NUMBER

9. SPONSORING / MONITORING AGENCY NAME(S) AND ADDRESS(ES)
U.S. Army Medical Research and Materiel Command
Fort Detrick, Maryland 21702-5012

10. SPONSORING / MONITORING AGENCY REPORT NUMBER

11. SUPPLEMENTARY NOTES

12a. DISTRIBUTION / AVAILABILITY STATEMENT
Approved for public release; distribution unlimited

12b. DISTRIBUTION CODE

13. ABSTRACT *(Maximum 200 words)*

Breast and diaphragm attenuation artifacts in SPECT 99mTc Sestamibi (MIBI) myocardial perfusion imaging are the source of decreased specificity of these studies. Same day stress and rest SPECT MIBI imaging, using the commercially available CEQual algorithm (CQL) which does not correct for attenuation, and a method which corrects for attenuation using simultaneous transmission/emission data from MIBI and a Gadolinium line source (STE), was performed on 58 normal women divided into 3 groups (normal, large breasted, and obese) and tracer distribution within the heart studied. There was no significant difference between groups for either STE or CQL. STE images demonstrated less pixel variability than CQL images. However, there was a significant difference ($p<.01$) in uniformity (homogeneity of tracer distribution) of myocardial distribution in the stress and rest images, with STE demonstrating improved uniformity (approximately 50%) in the anterior, anterolateral, septal, and inferolateral walls and slightly less uniformity in the inferoseptal wall, apex and mid-base. The inferolateral wall in STE images tended to show a reversible stress/rest defect, which may be misinterpreted as ischemia. Decreased tracer in the apex on STE images compared to CQL was seen, and may reflect a more accurate depiction of physiologic apical thinning. Areas of improved STE uniformity were seen in areas considered prone to attenuation artifacts.

CONCLUSION: STE generally results in less variable and more uniform images than non-attenuation corrected images. For STE, care should be exercise when interpreting the apex, where there is a tendency toward less tracer activity than expected, and in the inferolateral wall, where reversible defects were seen. There was no difference in uniformity in STE or CQL images when patients were stratified by breast size or body habitus.

14. SUBJECT TERMS	15. NUMBER OF PAGES
Defense Women's Health Research Program	24
	16. PRICE CODE

17. SECURITY CLASSIFICATION OF REPORT	18. SECURITY CLASSIFICATION OF THIS PAGE	19. SECURITY CLASSIFICATION OF ABSTRACT	20. LIMITATION OF ABSTRACT
Unclassified	Unclassified	Unclassified	Unlimited

FOREWORD

Opinions, interpretations, conclusions and recommendations are those of the author and are not necessarily endorsed by the U.S. Army.

____ Where copyrighted material is quoted, permission has been obtained to use such material.

____ Where material from documents designated for limited distribution is quoted, permission has been obtained to use the material.

____ Citations of commercial organizations and trade names in this report do not constitute an official Department of Army endorsement or approval of the products or services of these organizations.

N/A In conducting research using animals, the investigator(s) adhered to the "Guide for the Care and Use of Laboratory Animals," prepared by the Committee on Care and Use of Laboratory Animals of the Institute of Laboratory Resources, National Research Council (NIH Publication No. 86-23, Revised 1985).

X For the protection of human subjects, the investigator(s) adhered to policies of applicable Federal Law 45 CFR 46.

N/A In conducting research utilizing recombinant DNA technology, the investigator(s) adhered to current guidelines promulgated by the National Institutes of Health.

N/A In the conduct of research utilizing recombinant DNA, the investigator(s) adhered to the NIH Guidelines for Research Involving Recombinant DNA Molecules.

N/A In the conduct of research involving hazardous organisms, the investigator(s) adhered to the CDC-NIH Guide for Biosafety in Microbiological and Biomedical Laboratories.

Mike McBride 8/23/98

PI - Signature Date

Table of Contents

Evaluation of Breast and Diaphragm Artifact Using a Simultaneous Transmission/Emission Protocol for Attenuation Correction During SPECT 99mTc-Sestamibi Myocardial Perfusion Scans in Women Without Coronary Artery Disease

Mike McBiles, Albert Lambert, Dennis Stroud, Royce K. Solano, Sun Yung Kim; Fitzsimons Army Medical Center and Brooke Army Medical Center, Departments of Radiology, Nuclear Medicine Service

Myocardial perfusion imaging using radioactive tracers has gained widespread use in clinical practice for the evaluation of coronary artery disease. Its use is based upon the assumption that perfusion tracers, such as 99mTechnetium Sestabimi (MIBI), localize within the heart uniformly, albeit at different relative concentrations, when injected during exercise stress and in the resting state. Non-uniform accumulation is therefore the result of alterations in blood flow, most commonly due to coronary artery disease. The concept of stenosed coronary arteries causing focal decreased perfusion at stress and relative normalization of perfusion at rest has, as its clinical manifestation on MIBI imaging, decreased accumulation of tracer at stress and normal accumulation at rest when adjacent normal myocardium is used as a reference standard. Similarly, infarcted myocardium will demonstrate decreased or absent relative tracer uptake on both stress and rest images. These findings may be mimicked by artifacts caused by non-uniform attenuation of the gamma photon emitted from the perfusion tracer. The accuracy and adequacy of the diagnosis of coronary artery disease in women using myocardial perfusion imaging has been hampered by well-recognized artifacts caused by diaphragm, soft tissue, and breast attenuation[1 2 3 4 5]. The non-uniform attenuation almost always causes falsely decreased myocardial accumulation on perfusion imaging, and so has as its main effect decreases in specificity for myocardial disease. A recent meta-analysis of single photon emission computed tomography (SPECT) in radionuclide perfusion imaging reported an overall specificity of 64% [6], and specificity has been reported to be even less in women. Since non-invasive imaging is often used as a discriminator for subsequent invasive, costly and risky procedures, this lack of specificity is a serious problem in clinical practice. Quantification and characterization of the extent of these and other artifacts in MIBI SPECT myocardial studies has been poorly studied in women[7]. Although gender specific stress normal limits for same day rest/stress SPECT MIBI studies have been developed (the CEQual data base), large breasted women (greater than B cup) were excluded and obese women underrepresented [8]. Several authors have suggested that non-uniform attenuation correction may help to minimize attenuation artifacts[2 9 10]. Consequently, this study was designed to compare and characterize the artifacts generated in uncorrected SPECT MIBI images using a commonly used commercial program and data base called CEQual (CQL) with attenuation corrected images using a simultaneous transmission/emission (STE) protocol in women with a low likelihood of coronary artery disease stratified by breast size and body habitus.

MATERIALS AND METHODS

Patient Population

Fifty-eight non-pregnant women volunteers with less than a 5% probability of coronary artery disease [11] were recruited for this study in a protocol approved by the Institutional Review Board. Using the

New York Life Height and Weight Tables and answers to a questionnaire, women were prospectively assigned to three groups. Group A consisted of 23 women less than 10% above upper limits of normal weight for their height and weight, and with B cup bra size or less. Group B consisted of 17 women with bra cup size of C or greater. Group C consisted of women greater than 10% above the upper limits of normal weight for their height and weight. If a woman could be assigned to either group B or C, she was assigned to group B.

Exercise and Imaging Procedure

Patients were injected with 296 MBq 99mTc Sestamibi (Cardiolite, Dupont Pharma) and rest images obtained 1 hour later. Four hours after the rest injection, 814 MBq 99mTc-Sestamibi were injected during symptom limited graded exercise testing and stress images obtained 30 minutes later.

Imaging System and Acquisition Protocol

During both the stress and the rest imaging sessions, supine images with arms raised above head were obtained using a triple headed gamma camera (Picker Prism 3000, Cleveland, Ohio) with both high resolution parallel hole and high resolution fan beam collimators with a 20% window centered over the 140 kev photopeak. The order of collimators was randomly changed among patients. Imaging time was approximately 19 minutes at rest and 16 minutes at stress for both collimator types. When fan beam collimators were used, a Gadolinium-153 transmission line source was positioned at the collimator focal line of one camera head and an additional 100 kev photopeak with a 20% window acquired. With the parallel hole collimators, a 180 degree step-and-shoot protocol beginning at 45 degree LPO every 3 degrees for 60 images, magnification 1.3, 64X64 pixel matrix, 25 seconds per projection at rest and 20 seconds per projection at stress was used. With the fan beam collimators, a continuous acquisition 3 degrees per projection for 360 degrees, magnification 1.0, 64X64 pixel matrix, 10 seconds per projection at rest, 8.5 sec per projection at stress was performed.

Image Processing

Parallel hole collimators. The Cedar Sinai CEQual processing protocol was followed. Two dimensional pre-filtering with a Butterworth filter, order 5, Nyquist cutoff .25 for rest and order 2.5, cutoff .33 for stress studies, followed by transaxial tomogram reconstruction using a ramp filter to a pixel thickness of 6.4 mm was accomplished.

Fan beam collimators. Images from identical angles on all three heads in all 3 heads were summed in both energy windows for 120 projections, technetium downscatter into the 100 kev window corrected on the head opposite the gadolinium line source, and an attenuation map derived using an iterative maximum likelihood algorithm. The 140kev emission data were then simultaneously reconstructed and attenuation corrected using a 20 iteration maximum likelihood reconstruction algorithm and zoomed with an appropriate factor to a 6.4mm pixel size. The images were then filtered with a 3 dimensional Fourier filter using the same cutoff and order as the parallel hole collimator studies.

Reformatting and normalization. Using the transaxial images from both collimator types at rest and stress, the long axis of the heart was determined, short axis slices reformatted, and adjacent slices added in staggered summation to a slice thickness of 12.8mm. The resultant data were then reformatted into a myocardial volume map containing a total of 480 pixels as per the CEQual formalism[8]. Briefly, after reformatting the short axis data into 480 voxels, a scale factor was generated by determining the most normal territory in the patient's heart as the area with the highest activity ratio compared with a comparable area in the normal data base. All pixels were normalized by this scale factor. The pixels were then

redisplayed into 12 profiles, consisting of 8 mid and basal cylindrical slices and 4 apical spherical slices (numbered 1-12, apex to base), each with 40 radial sectors (which run radially counterclockwise from 12 o'clock, with 10, 20, 30 and 40 roughly corresponding to septum, inferior, lateral, and anterior walls respectively).

Statistical Analysis

To (1) identify for CQL and STE methods those regions of the heart with the greatest variability within and between patients and (2) compare CQL and STE across groups A, B, and C, an analysis of variance using the median polish algorithm described by Tukey[12] on patient, sector, profile, and residual effects was performed. Multiple combinations of these interactions were also considered, and analysis was repeated on stress, rest, and stress minus rest images (stress-rest). This generated an analysis of variance table for each of stress, rest, and stress-rest data sets for the 58 volunteers nested within 3 groups and crossed with 2 acquisition/processing methods, 40 radial sectors and 12 short axis profiles. The methods of acquisition and processing, profiles, sectors, patient group, and intra-patient variation were treated as random variables for the purpose of analysis of variance. Uniformity of tracer distribution throughout the heart is assumed.

RESULTS

Stress image data set

There was no difference in normalized median pixel activity among the three groups ($p=.52$), or between CQL and STE ($p=.47$). As expected, given attenuation as a significant factor, a large source of the uniformity variation in median pixel value is due to the pixel location within the heart, with the greatest variation due to axial location (apex and base), followed by radial location (inferior and anterior wall) for both technologies (Fig. 1,2). A highly significant difference in uniformity between CQL and STE methods exists ($p<.001$), with more uniformity (tendency toward unity) in the STE method than CQL in the anterior, and septal, and inferolateral walls, similar uniformity in the mid ventricle, anteroseptal, inferior and lateral walls and base, and slightly less uniformity at the inferoseptal wall, mid heart and apex (Fig. 1,2). In almost all areas, STE was less variable than CQL in sectors (SD range.003 to .055 vs. .05 to .06, $p<.001$) (Fig. 3), profiles (SD range.01 to .06 vs. .01 to .1, $p<.01$)(Fig. 4), and in residual (unaccounted) effects (average SD .04 vs. .05). Uniformity in profile slices between groups as a function of STE or CQL did not reach significance ($p=.19$), but uniformity due to sector variation did ($p<.01$). The uniformity improvement for STE over CQL is mainly due to improvement in the anterolateral and septal walls, and despite STE relative decrease in uniformity in the inferior wall (Fig. 5,6).

Rest image data set

Similar results were found for the rest images. There was no significant difference in median pixel activity among the three groups ($p=.91$) or between CQL and STE ($p=.2$). Again, highly significant differences in uniformity were seen between the CQL and STE methods ($p<.001$) with STE more uniform in the anterior, septal, inferolateral, and anterolateral walls and base, similar uniformity in the anteroseptal and lateral walls, and slightly less uniformity in the inferoseptal wall, apex and mid heart to base (fig 7,8). In most areas, STE was significantly less variable than CQL in sectors and (SD range.003 to .065 vs. .05 to .08, $p<.001$) (Fig. 9), less variable in profiles (SD range.03 to .065 vs. .04 to .1, $p<.01$) (Fig. 10), and in

residual (unaccounted) effects (average SD .045 vs. .051). As with the stress data, uniformity differences due to profile slices between groups using STE and CQL was not significant (p=.39), but sector variation was (p<.001)(Fig. 11,12), with the uniformity improvement being in the anterolateral and septal walls, and despite a small STE relative decrease in uniformity in the inferior wall (Fig. 5,6).

Stress minus rest data set

There was no significant difference in mean pixel activity among the three groups (p=.71) but differences between CQL and STE were highly significant (P<.001)(Fig. 13). There were significant uniformity differences in both sectors and profiles (p<.001, p=.01), with the contribution of CQL and STE to uniformity significant for sectors (p<.001), and barely non-significant for profiles (p=.06) (Fig. 14,15). Those areas differing in uniformity from zero by more than two standard deviations are the septum, inferolateral, and anterolateral wall, and apex for STE and anteroseptal, inferoseptal wall, mid apex and base for CQL. Variability for STE is significantly less than CQL in profiles (SD range .05 to .02 vs. .1 to .02, p<.01) and is also significantly less for STE than CQL in almost all sectors (SD range.02 to .05 vs. .04 to ..06, p<.001) (Fig. 16,17).

DISCUSSION

In stress studies, areas of greater uniformity on the stress STE studies correspond roughly to areas of expected breast and diaphragm attenuation, indicating a probable positive effect of the attenuation correction algorithm on these areas. The approximate uniformity improvement is 50% in the anterior and anterolateral walls and inferolateral walls for STE. This likely would improve the false positive rate for defects in these areas, as confirmed by others[9 13]. Of interest, however, is that these same areas also show significant (greater than 2 SD) positive non-uniformity on stress-rest STE images. Since the corresponding areas in the stress-rest STE images display less uniformity (although other areas show greater uniformity than CQL), it may be that other factors are causing either over-correction at stress or under-correction at rest in the attenuation correction algorithm, such as insufficient volume sampling causing truncation of the data set with fan beam collimators, or increased liver activity causing distortion of the attenuation map[14 15 16]. Although not studied here, this phenomenon may be of less importance in clinical practice, since greater uniformity and less variability of STE images may be masked by compression of these differences into a smaller area in the upper end of the gray scale during image interpretation. The positive pixel difference in the stress-rest data is not likely to be a clinical concern in the septum, anterior and lateral walls and is unlikely to result in misinterpretation of the images, since this "hot" stress "cold" rest pattern is probably not going to be interpreted as a pathologic abnormality. However, the reverse pattern in the inferolateral wall may be misinterpreted as ischemia.

In the stress and rest images, STE appears to produce more uniform images than CQL, with the exception of a small area near the apex, mid ventricular slices, and inferoseptal walls. The decrease in activity at the apex of the heart on STE images has been noted by others[9], and has been attributed to a more accurate representation of a true physiologic thinning of the apex of the heart. Clinical image interpreters who are used to traditional reconstruction algorithms should be aware of this effect and not misinterpret it as a true defect. The remaining uniformity differences are relatively small compared to large uniformity variations in CQL images, for example, in the anterolateral wall. Greater uniformity in areas of expected attenuation artifact is indirect evidence of some success of this algorithm. However, due to the inherent significant differences in acquisition and processing between STE and CQL some other factor may be responsible for this change in uniformity. We attempted to keep as many acquisition and processing factors

as constant as possible, including acquisition time and total emission counts, processing filter, and pixel size in order to minimize this possibility. The STE images are less variable, implying greater pixel homogeneity as a group, when compared to the CQL images in almost all sectors and profiles. While this may be due to a greater precision of the STE process, a hidden mathematical smoothing in the complex STE algorithm may also account for this phenomenon. This effect was confirmed visually by the image interpreters, who noted a distinct difference in the quality of the STE images, which generally appeared smoother.

Of particular interest in this study is that grouping of women into specific categories (normal, large breasted, obese), which would be expected to accentuate significant differences in the in two acquisition and processing technologies, did not result in a demonstrable difference between these groups for either technologies in either the stress, rest images or stress-rest images. While this may be due to a lack of statistical power due to the number of women in each subgroup, it may also suggest that other factors present in all groups overshadow these effects. It may be breast density and not size is more important[17]. The heterogeneity of the attenuation and not he absolute amount may the more critical factor. Inspection of Figures 5,6,11, and 12 reveals no areas of difference where any group is clearly different from others.

An attempt was made to qualitatively compare STE and CQL images in terms of a semi-quantitative observer grading system which has been used by others[8] in determining the degree of abnormality of myocardial segments. However, it was realized early in this investigation that observers could almost always distinguish CQL images from STE images by differences in apparent background noise and image smoothness, an effect which was not investigated in this study. Since an unblinded comparison would be meaningless, and because normal observer thresholds were by necessity generated from the older CQL technology, this approach was abandoned. A more valid approach would be to generate receiver-operator characteristic curves for the STE technology using both normal and abnormal patients. Given the differences between the significant differences between the two methods of data acquisition as demonstrated in normals in this study, this is an area which should be studied, since the effect of STE on an abnormal population is not known.

Conclusion

STE results in greater uniformity in those areas of the heart most commonly associated with attenuation artifacts in women when compared with non-attenuation correction methods which are now in common use in clinical practice. Greater uniformity in areas of known attenuation artifact may increase the specificity of myocardial perfusion imaging, and this technology deserves consideration for routine adoption in clinical practice. However, care should be exercised in the inferoseptal and apical walls where there is greater non-uniformity in STE when compared with CQL images. In addition, the inferolateral wall abnormalities may be interpreted as ischemia because this area tends to appear more intense on rest imaging when STE is used. The STE apical non-uniformity may be a true physiologic finding; the inferoseptal non-uniformity may be a result of adjacent extra-cardiac activity not adequately handled by the STE algorithm.

No significant difference for either algorithm could be demonstrated in any area of the heart when women were stratified by breast size or obesity, and STE resulted in improved attenuation correction for all groups in the areas of expected attenuation artifact.

REFERENCES

[1] Garver PR, Wasnich RD, Shibuya AM, Yeh F. Appearance of breast attenuation artifacts with thallium myocardial SPECT imaging. Clin Nucl Med 1985, 10(10):694-6.

[2] Goodgold HM, Rehder JG, Samuels LD, Chaitman BR. Improved interpretation of exercise Tl-201 myocardial perfusion scintigraphy in women: characterization of breast attenuation artifact. Radiology 1987, 165(2):361-6.

[3] Botvinick EH. Breast attenuation artifacts in Tl-201 scintigraphy [letter]. Radiology 1988, 168(3):878-9.

[4] Wang SJ, Chen YT, Hwang CL, Lin MS, Kao CH, Yeh SH, 99mTc-sestamibi can improve inferior attenuation of Tl-201 myocardial SPECT imaging. Int J Cardiac Imaging 1993, 9(2):87-92.

[5] Lette J, Caron M, Cerino M, McNamara D, Metayer S, D'Aoust S, Eybalin MC, Levesseur A, Gregoire J, Arsenault A. Normal quantitative and qualitative Tc-99m sestamibi myocardial SPECT: spectrum of intramyocardial distibution during exercise and at rest. Clin Nucl Med 1994, 19(4):336-43.

[6] Fleischman KE, Hunink MG, Kuntz, KM, Douglas PS. Exercise echocardiography or exercise SPECT imaging? A meta-analysis of diagnostic test performance. JAMA 1998; 280:913-920.

[7] Toft J, Hesse B, Rabol A. The occurrence of false positive technetium-99m sestamibi bull's eye defects in different reference data bases. Eur J Nucl Med 1997, 24(2):179-83.

[8] van Train KF, Areeda J, Garcia EV, Cooke DC, Maddahi J, Kiat H, Germano G, Silaga G, Folks R, Berman D. Quantitative same-day rest-stress technetium-99m-sestamibi SPECT: definition and validation of normal limits and criteria for abnormality. J Nucl Med 1993; 34:1494-1502.

[9] Ficaro EP, Fessler JA, Ackermann RJ, Rogers WL, Corbett JR, Schwaiger M. Simultaneous transmission-emission thallium-201 cardiac SPECT: effect of attenuation correction on myocardial tracer Distribution. J Nucl Med 1995; 36:921-931.

[10] Grover-McKay M. Gender related imaging issues in assessment of coronary artery disease by nuclear techniques. American J Cardiac Imaging 1996; 10(1):54-64.

[11] Diamond GA, Forrester JS. Analysis of probability as an aid in the clinical diagnosis of coronary artery disease. N Engl J Med 1979; 300:1350-1358.

[12] Tukey JW. Exploratory Data Analysis. Addison-Wesley, Reading, Massachusetts (1977)

[13] Ficaro EP, Fessler JA, Shreve PD, Kritzman JN, Rose PA., Corbett JR. Simultaneous transmission/emission myocardial perfusion tomography: diagnostic accuracy of attenuation corrected 99mtc-sestamibi single-photon emission computed tomography. Circulation 1996; 93:463-473.

[14] Heller EN, Deman P, Liu P, Dione D, Zubal G, Wackers FJ, Sinusas AJ. Extracardiac activity complicated quantitative cardiac SPECT imaging using a simultaneous transmission-emission approach. J Nucl Med 1997; 38:1882-1890.

[15] Nuyts J, Dupont P, Van den Maegdenbergh V, Vleugels S, Suetens P, Mortelmans L. A study of the liver-heart artifact in emission tomography. J Nucl Med 1995; 36:133-139.

[16] King MA, Xia W, deVries DJ, Pan TS, Villegas BJ, Dahlberg S, Tsui BM, Ljungberg MH, Morgan HT. A Monto Carlo investigation of artifacts caused by liver uptake in single-photon emission computed tomography perfusion imaging with technetium 99m-labeled agents. J Nucl Cardiololgy 1996, 3(1):18-29.

[17] Cohen M, Touzery C, Cottin Y, Benoit T, d'Athis P, Louis P, Wolf JE, Rigo P, Brunotte F. Quantitative myocardial thallium single-photon emission computed tomography in normal women:demonstration of age related differences. Eur J Nucl Med 1996, 23(1):25-30.

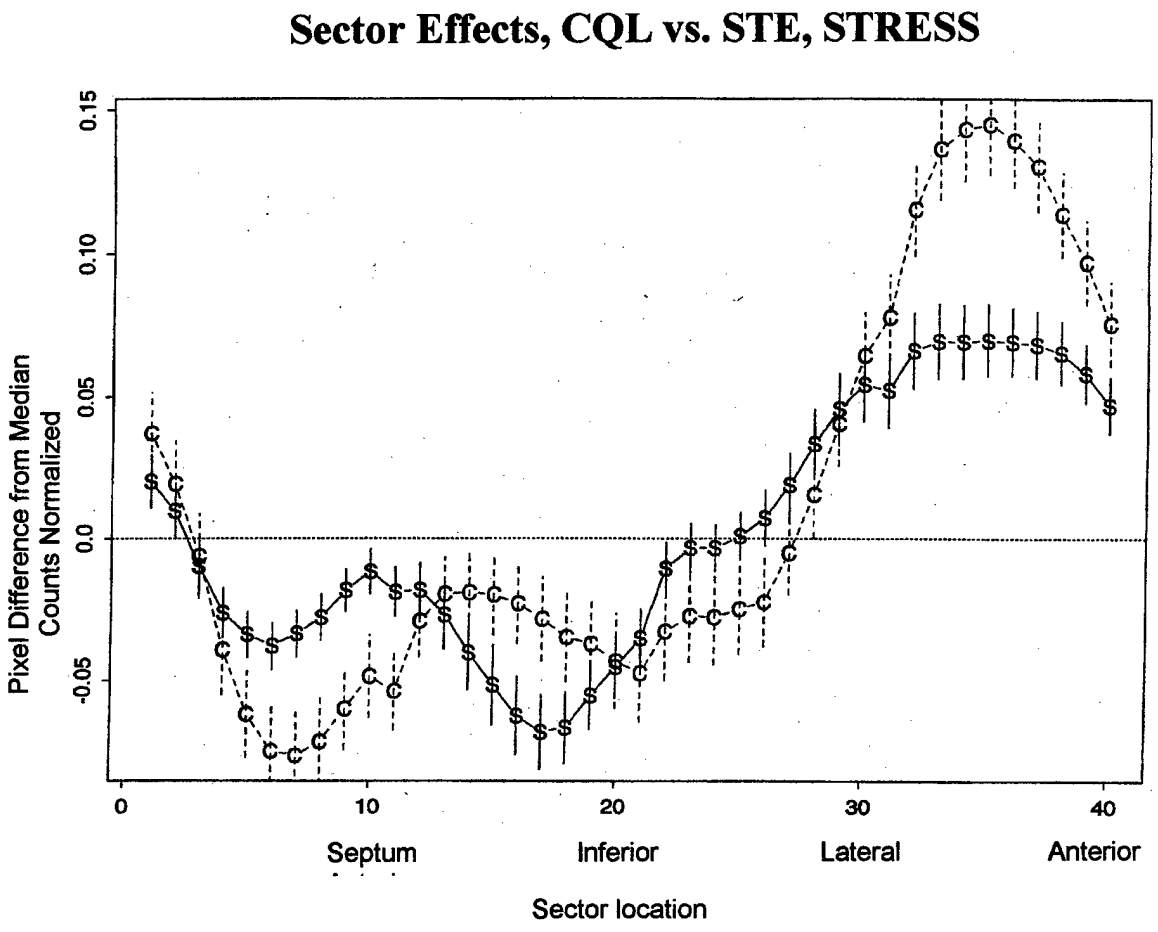

Figure 1. Pixel Value averaged over 58 patients, shown with limits of 2 standard deviations. S=STE, C=CQL, Stress.

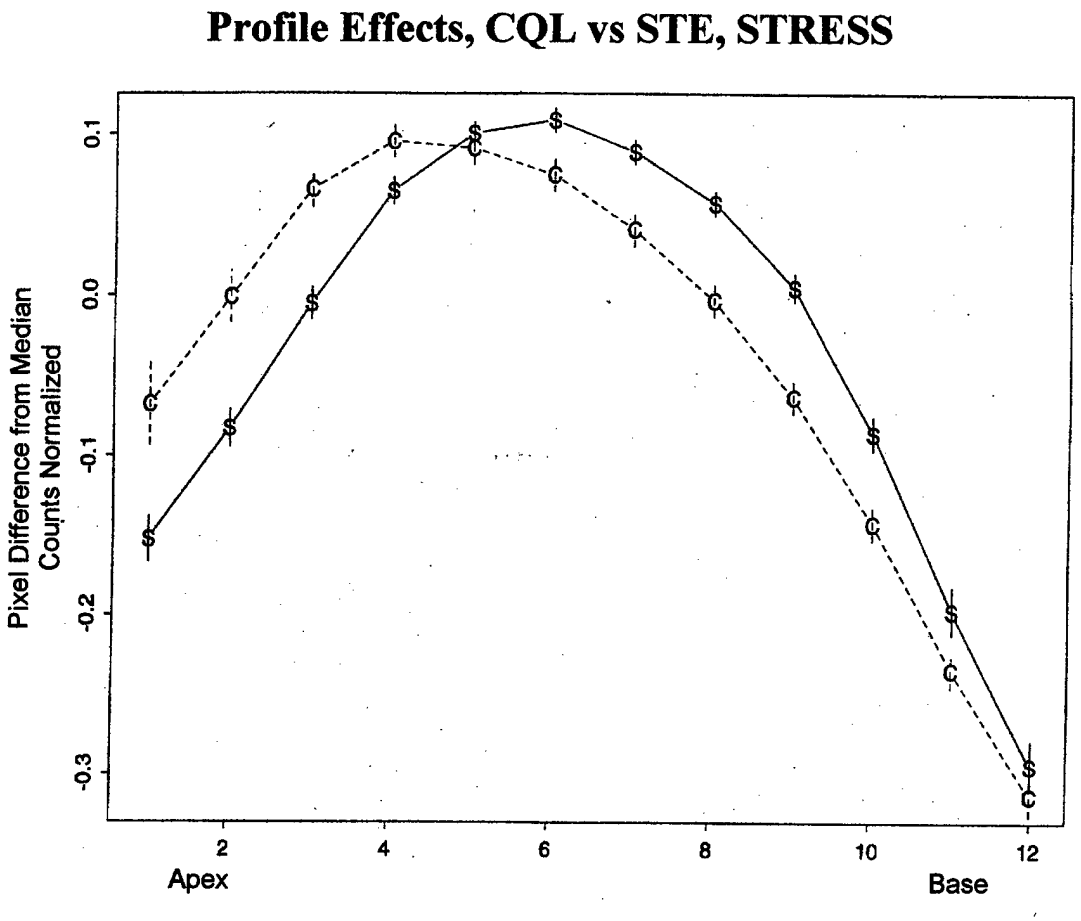

Figure 2. Pixel Value averaged over 58 patients, shown with limits of 2 standard deviations. S=STE, C=CQL, Stress

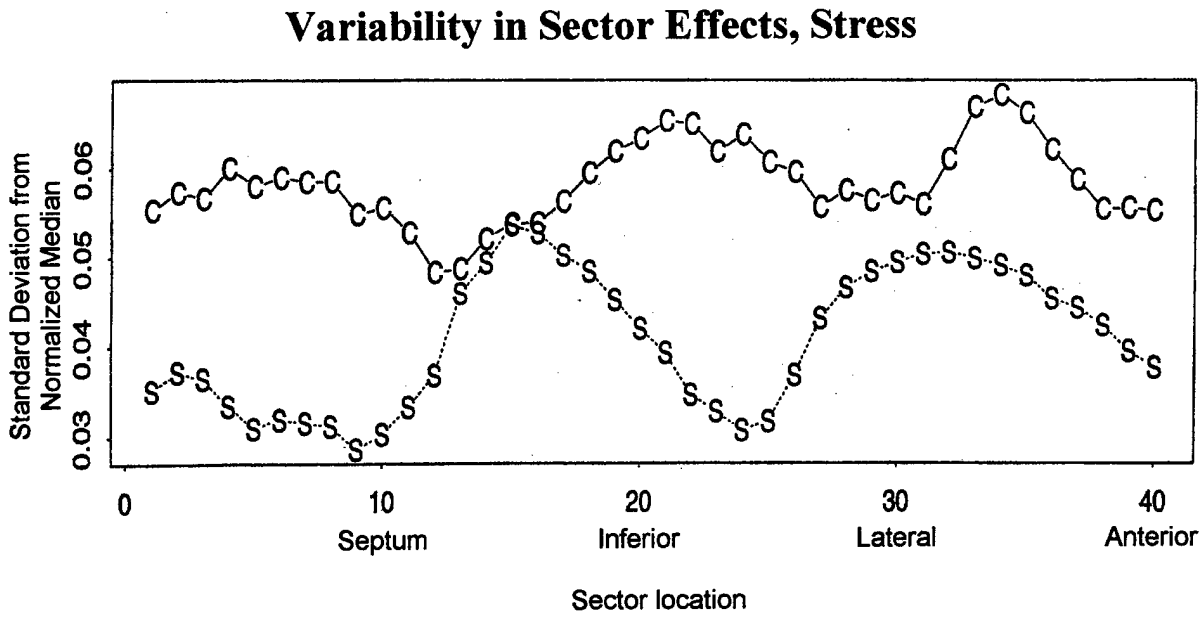

Figure 3. Standard deviation of sector effects for CQL (C) and STE (S), Stress.

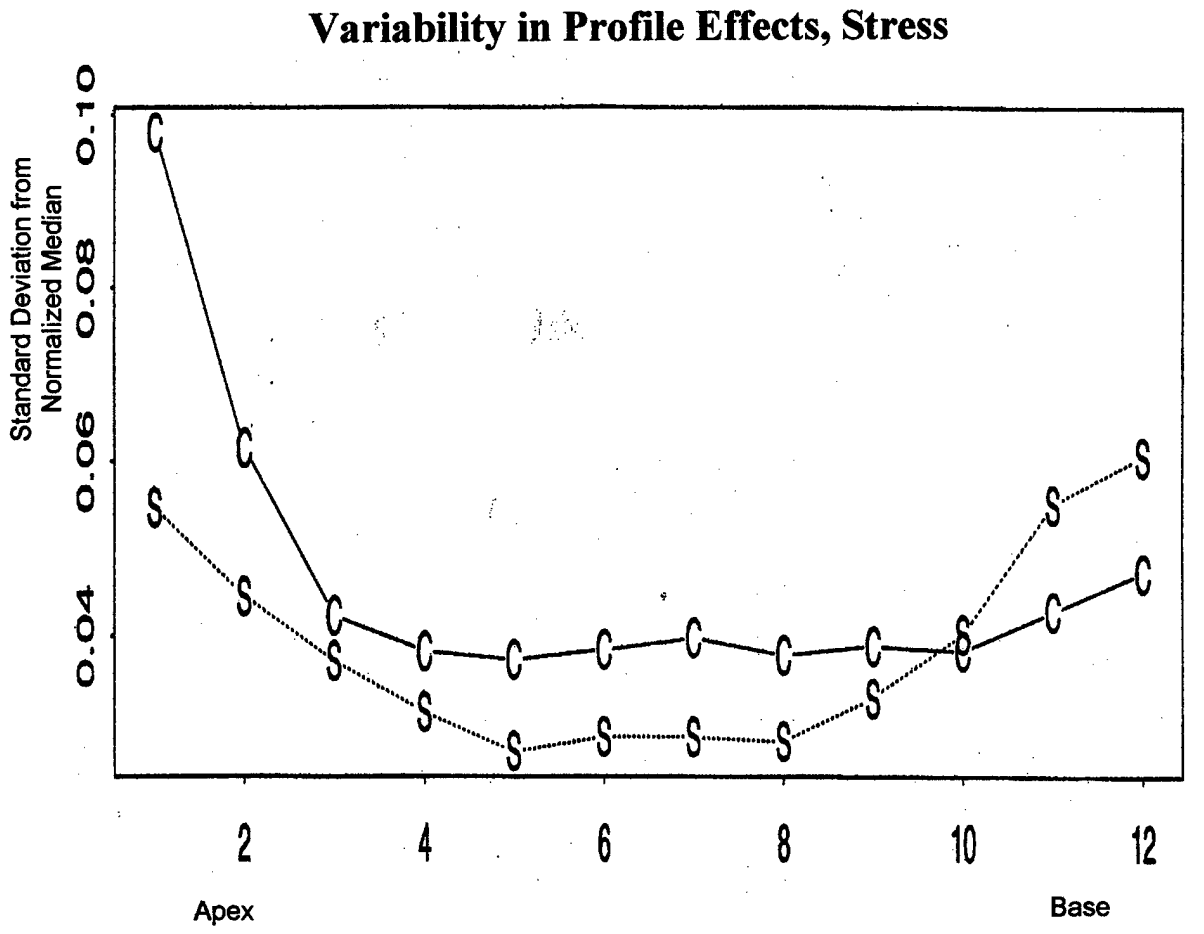

Figure 4. Standard deviation of profile effects for CQL (C) and STE (S), Stress.

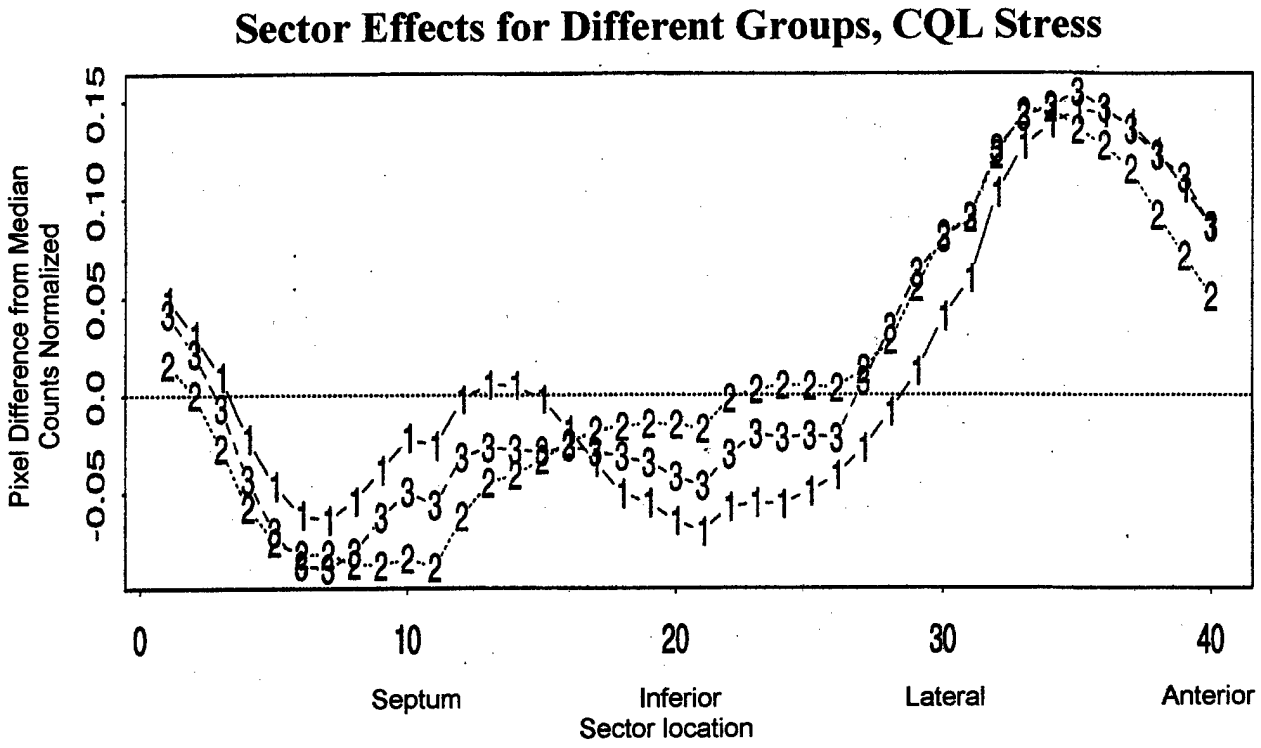

Figure 5. CQL Sector Effects by Patient Group, Stress. 1=Normals, 2=greater than B-cup, 3=Obese

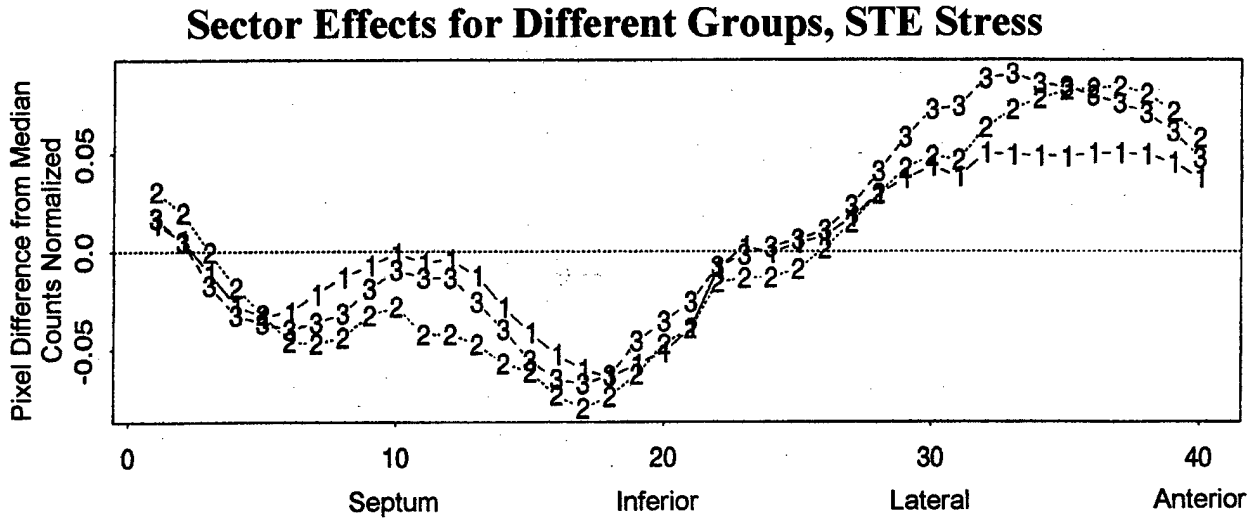

Figure 6. STE Sector Effects by Patient Group, Stress. 1=Normals, 2=greater than B-cup, 3=Obese

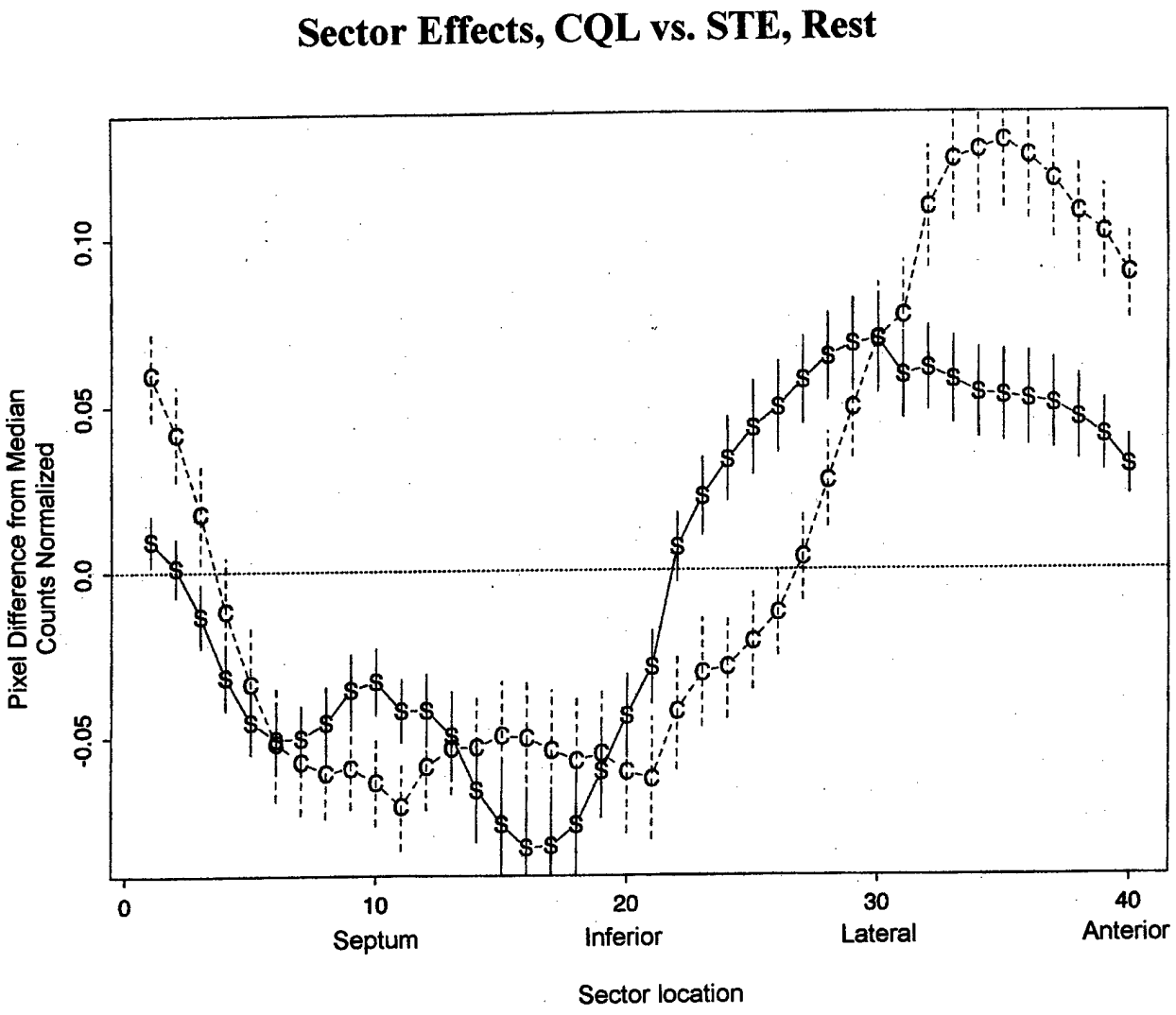

Figure 7. Pixel Value averaged over 58 patients, shown with limits of 2 standard deviations. S=STE, C=CQL, Rest.

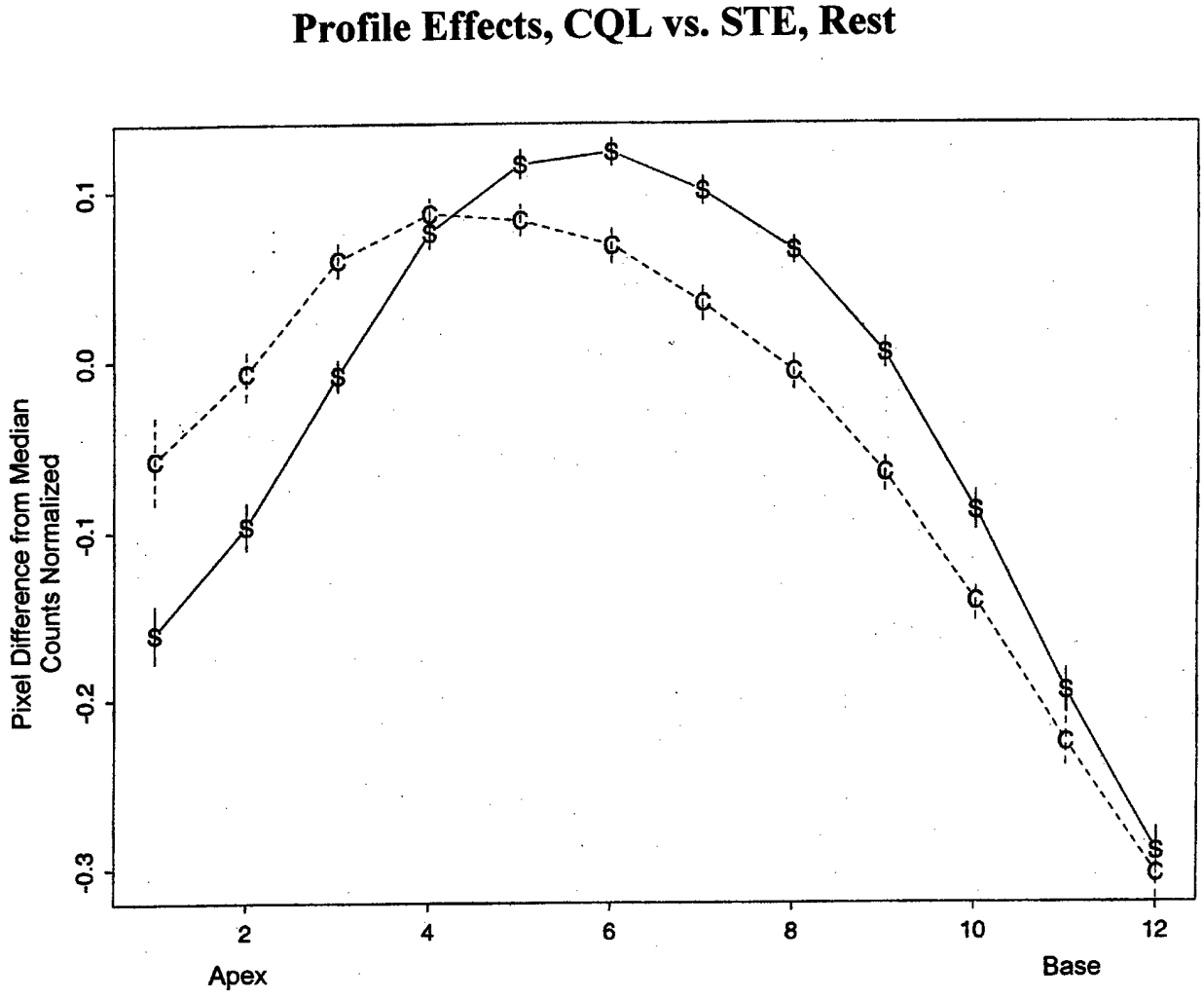

Figure 8. Pixel Value averaged over 58 patients, shown with limits of 2 standard deviations. S=STE, C=CQL, Rest.

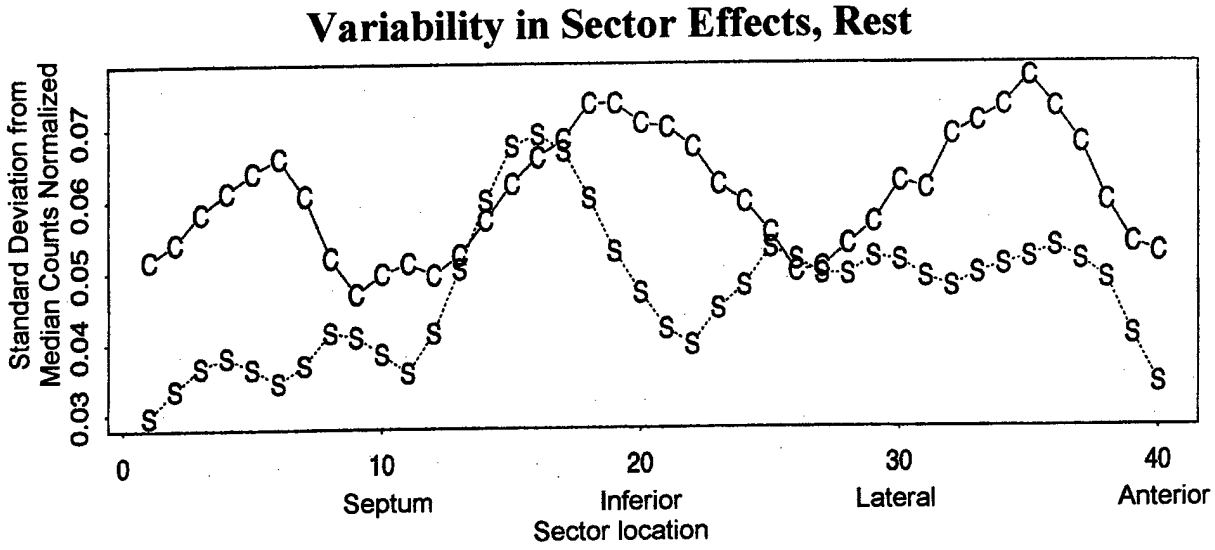

Figure 9. Standard deviation of sector effects for CQL (C) and STE (S), Rest.

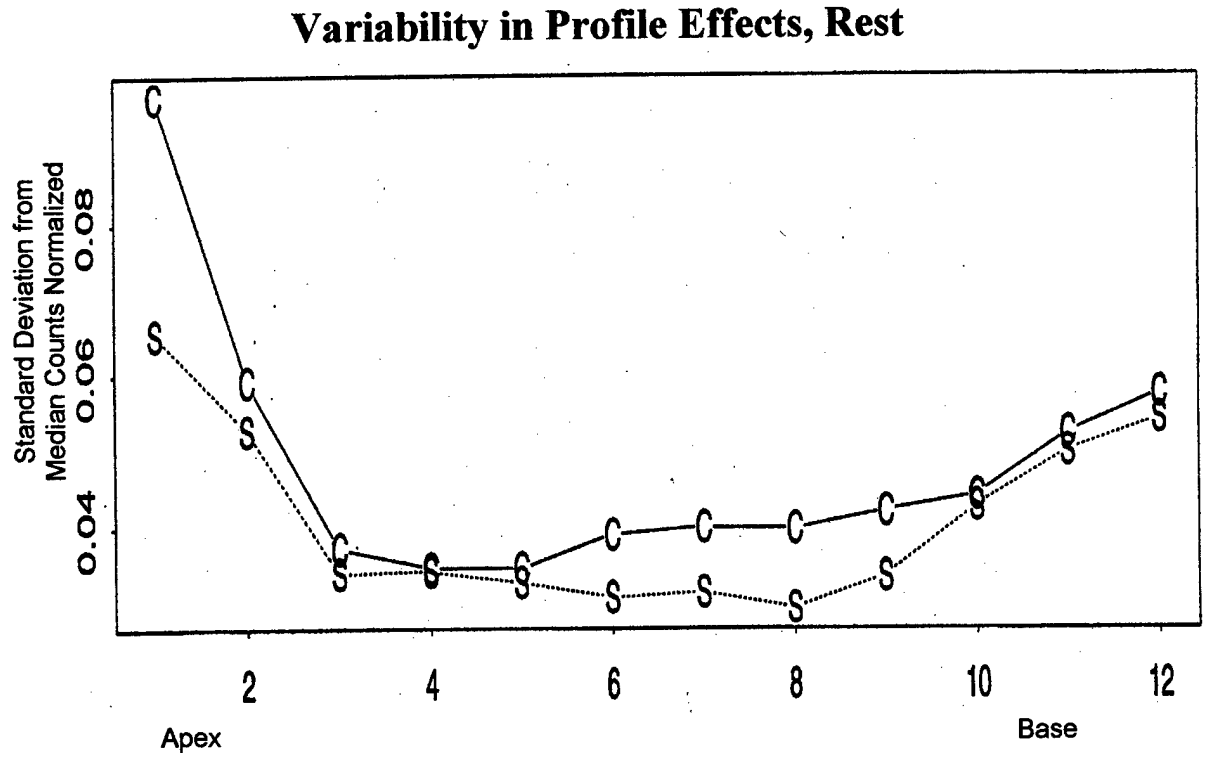

Figure 10. Standard deviation of profile effects for CQL (C) and STE (S), Rest.

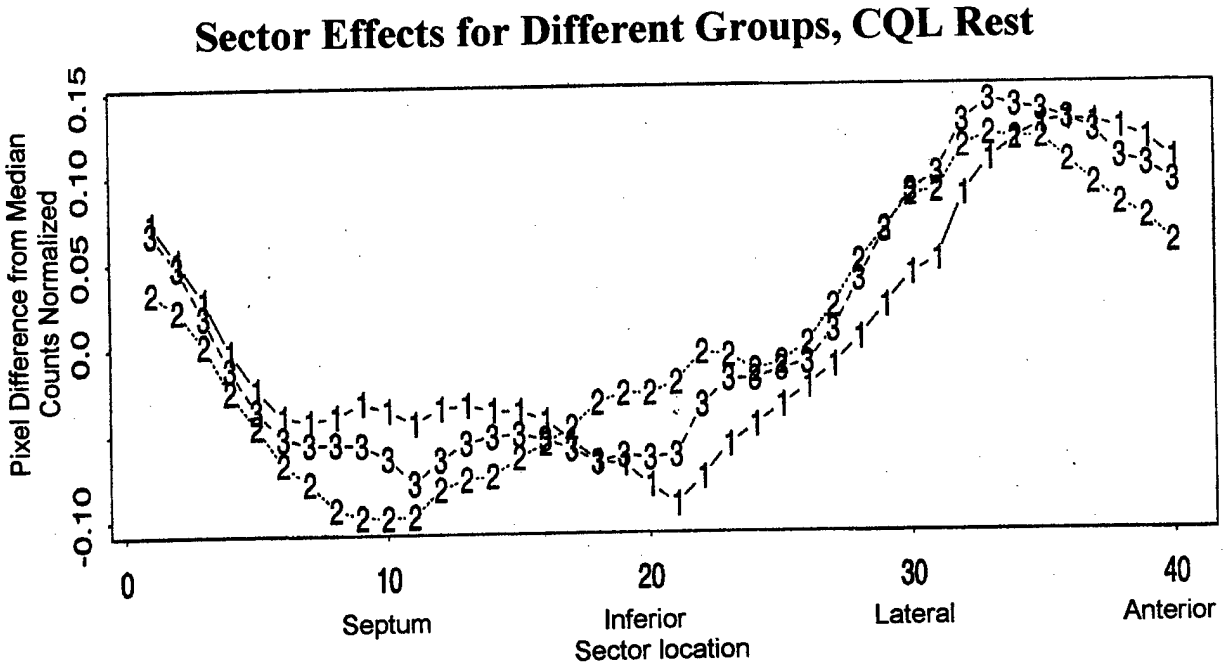

Figure 11. CQL Rest Sector Effects by Patient Group. 1=Normals, 2=greater than B-cup, 3=Obese

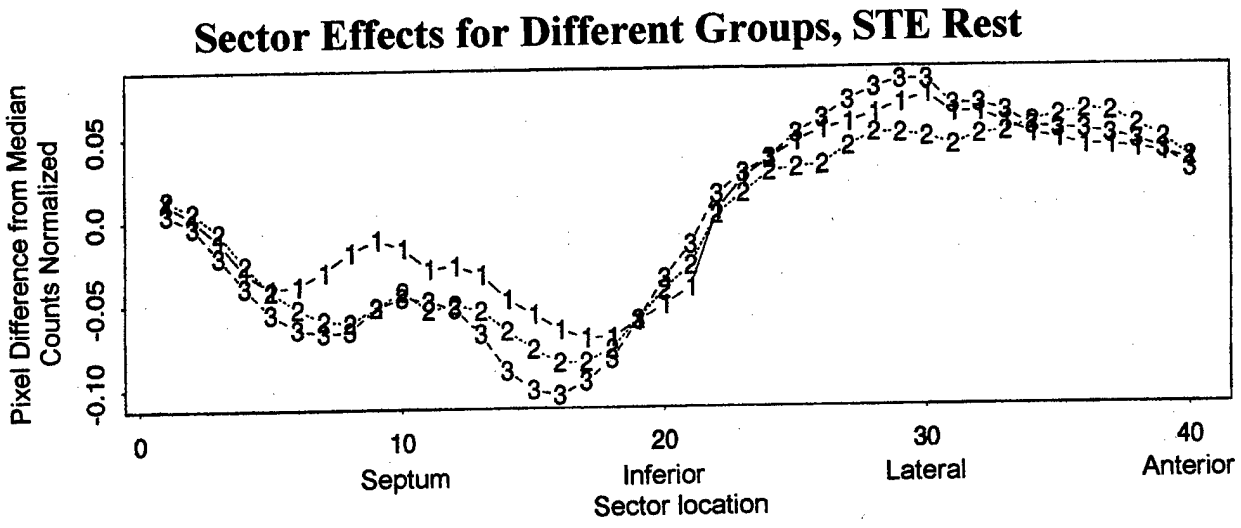

Figure 12. STE Rest Sector Effects by Patient Group. 1=Normals, 2=greater than B-cup, 3=Obese

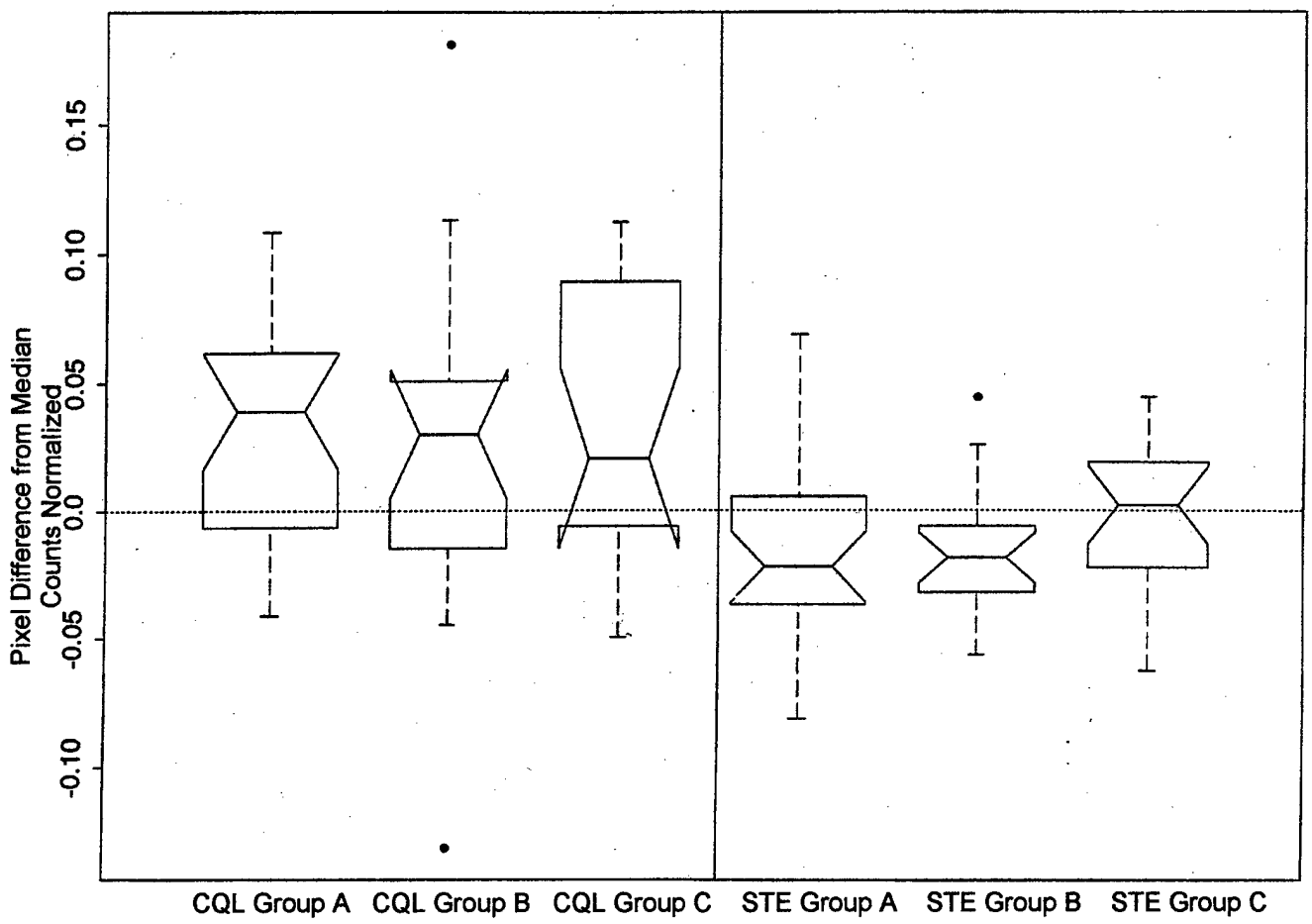

Figure 13. Stress minus Rest, Effect of Group and Acquisition Method. Notched box plots show significant differences between groups as a function of acquisition method between CQL and STE Groups A and B (shoulder of the notches do not overlap, $p<.05$)

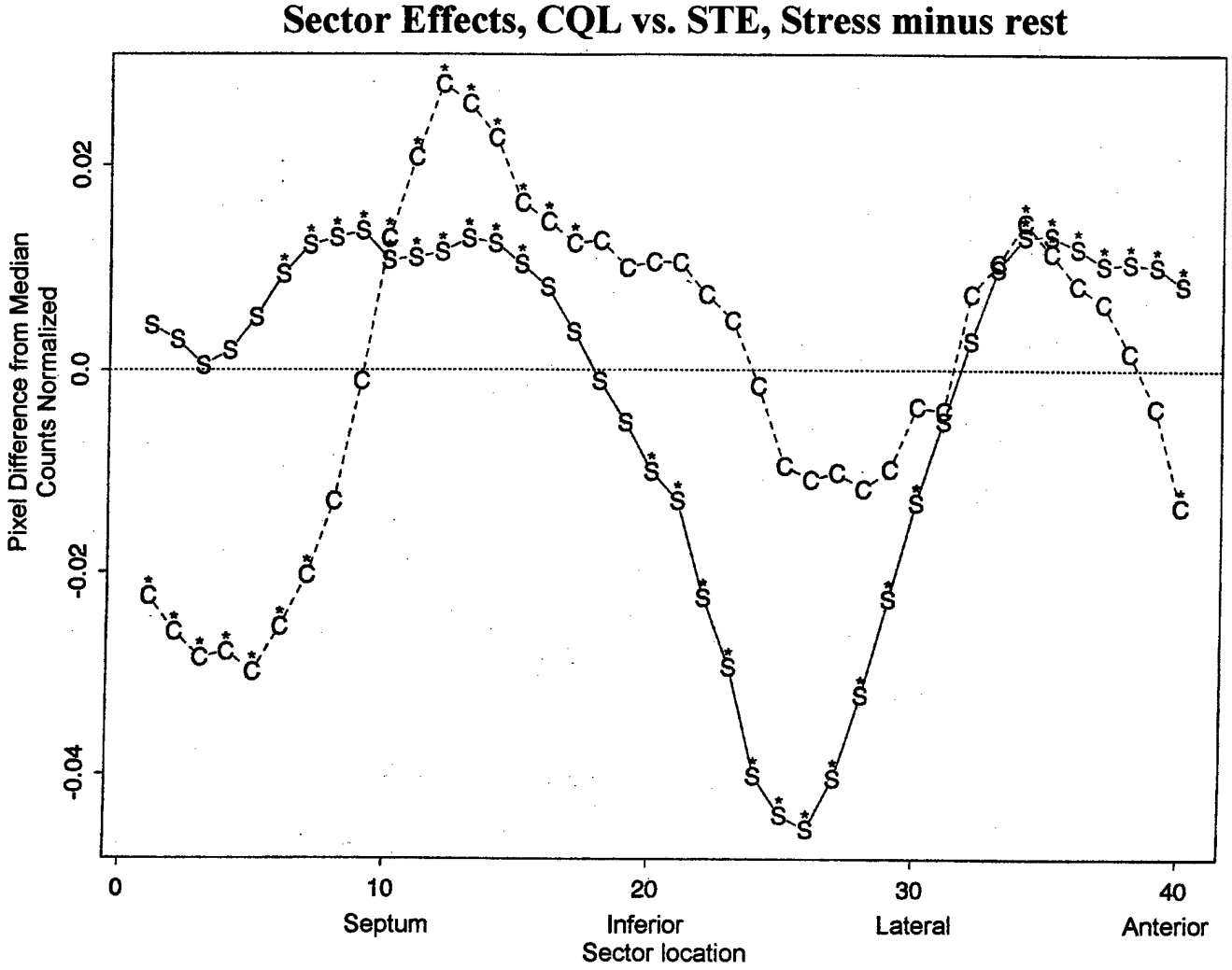

Figure 14. Stress minus rest sector effect. * indicates effect differs from zero by more than 2 standard errors. C=CQL, S=STE

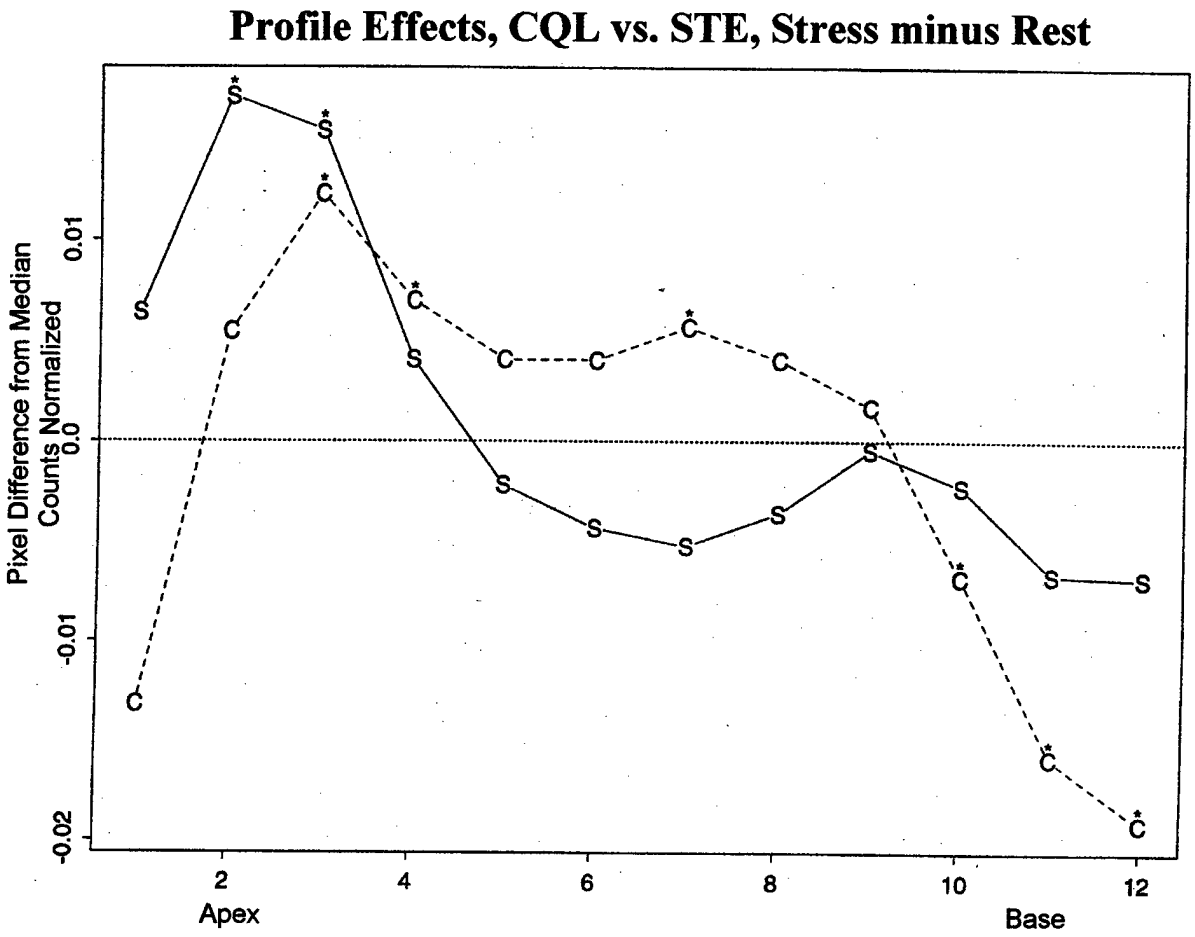

Figure 15. Stress minus rest profile effect. * indicates effect differs from zero by more than 2 standard errors. C=CQL, S=STE

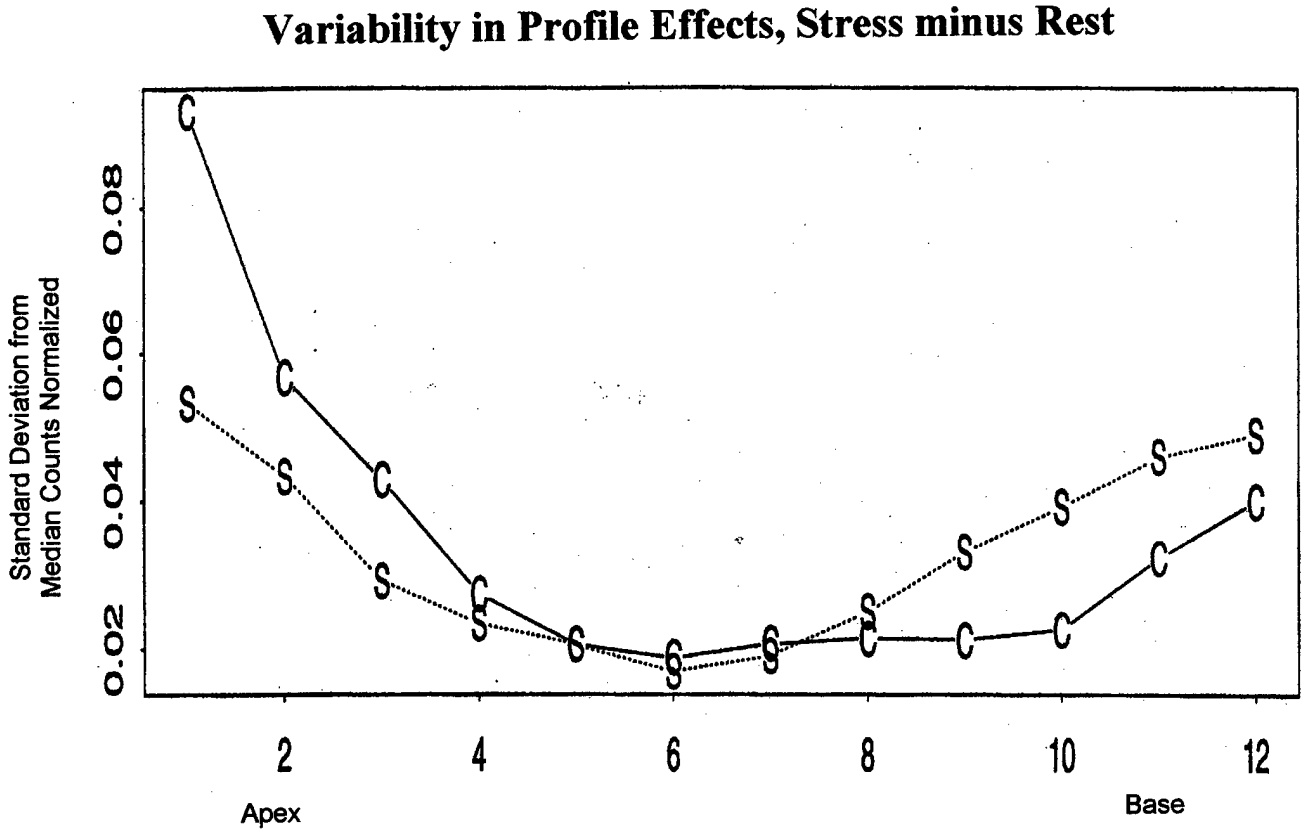

Figure 16. Standard deviation of profile effects for CQL (C) and STE (S), Stress minus rest.

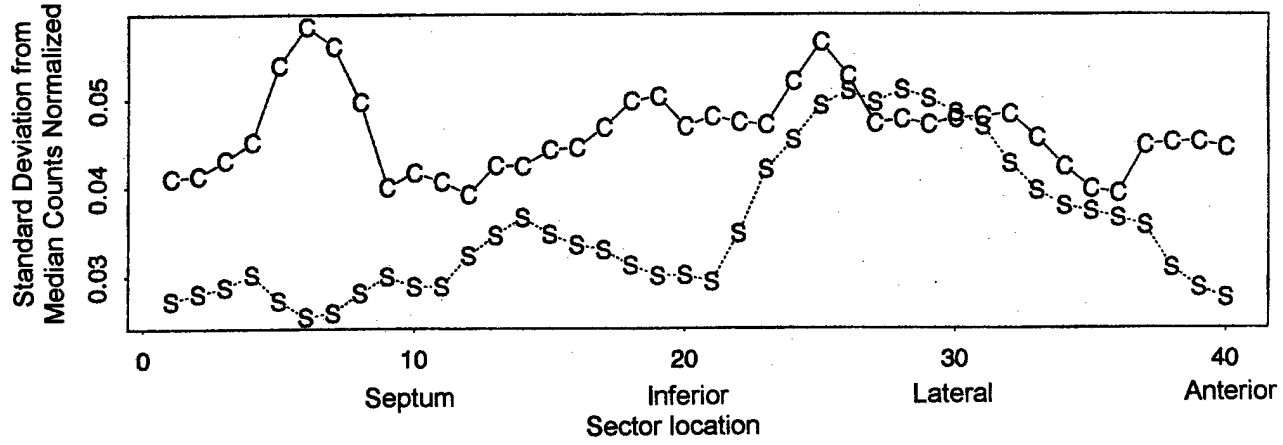

Figure 17. Standard deviation of sector effects for CQL (C) and STE (S), Stress minus rest.

List of personnel receiving Salary

Karen Kafadar, Colorado State University Department of Mathematics

James Koehler, Colorado State University Department of Mathematics